N87-23314

FORMATION MECHANISMS OF LABORATORY DOUBLE LAYERS

Chung Chan
Center for Electromagnetics Research
and
Department of Electrical and Computer Engineering
Northeastern University
Boston, Massachusetts 02115, U.S.A.

ABSTRACT

The evolution processes of double layers have been studied in a series of laboratory experiments. It was found that the existence of virtual cathode-type potential wells at the electron injection boundary was the dominant triggering mechanism. The rapid growth of the potential well led to collisionless ion trapping and the establishment of the necessary trapped ion population. For double layers with small potential drops, collisionless ion trapping actually induced ion-ion streaming instabilities and the formation of ion phase-space vortices. In this regime, the system often exhibited relaxation-type oscillations which corresponded to the disruption and the recovery of the double layers.

I. INTRODUCTION

Much of our recent understanding of double layers has come from laboratory experiments and numerical simulations which had rather limited system dimensions. The system boundaries are often in close proximity with the double layer electric field, thus affecting almost all aspects of double layer physics. The situation is obviously different in space plasmas where boundaries are not well defined and often far away from the regions of possible double layer formation. In order to extrapolate the results from laboratory and computer experiments to the space context, it is important to understand the role of the system boundaries on the formation of double layers.

Most double layers experiments (Quon and Wong, 1976; Leung et al., 1980; Singh and Schunk, 1983; Iizuka et al., 1979; Saeki, et al., 1980) have utilized the injection of a drifting electron species to trigger the formation process. It was found that a necessary condition for double layer formation is that the electron drift velocity v_d exceed the thermal velocity v_{te} of the ambient electrons. This condition results in the belief that the Buneman instability with an instability threshold of $v_d \geq v_{te}$ was the triggering mechanism for double layers. However, double layers with potential drops $\Phi > T_e/e$, the electron temperature divided by the electron charge, have been observed (Hollenstein et al., 1980) experimentally with v_d as small as $0.2\, v_{te}$. Ion-acoustic turbulence instead of the Buneman instability was expected to be the triggering mechanism for double layer formation in that experiment.

Numerical simulation (Sato and Okuda, 1980) of double layers with $v_d \leq v_{te}$ have found different results. No double layers with $\phi > T_e/e$ were found. Rather, a new class of double layers with non-montonic potential profiles and $\phi \leq T_e/e$ was found. These double layers were always preceded by negative potential pulses and associated with current-driven, ion-acoustic turbulence. As such, these double layers have been identified as "ion acoustic" in order to distinguish them from the conventional double layers. Since an electron drift velocity of $v_d > v_{te}$ may not exist in space (e.g., the auroral plasma), the ion-acoustic double layers have also become a subject of considerable interest.

In this talk, we will discuss previous (Hershkowitz et al., 1981) as well as new experimental results in order to identify the formation mechanism of double layers in our triple plasma device. We begin with the roles of the

boundaries on the steady state characteristics of double layers. It is shown that the drifting electrons provide the initial space charge for double layer formation, while the trapped ions determine the evolution process and the shape of the potential profile. It is also shown that the growth of virtual cathode-type potential wells at the electron injection boundary is the triggering mechanism for double layers. Collisionless ion trapping by the potential well is found to be the main process for the establishment of the necessary trapped ion population.

Furthermore, double layers with $\phi \leq T_e/e$ are shown to be unstable to the evolution of ion phase-space vortices from ion-ion streaming instabilities. In this regime, the double layer potential profile has a strong resemblance to ion-acoustic double layers. This result may represent an alternative explanation of the small electric field signatures observed in the auroral plasma.

II. STEADY STATE EXPERIMENT

It is useful to first describe the operational characteristics of the triple plasma device in order to get some insights into the sources of particles that support the double layer. The triple plasma device consists of two source plasmas bounding a target plasma. Each source is separated from the target chamber by two grids. Plasma potential in each chamber is determined by the bias voltages of the grid and the internal anode. The source plasmas are created by filament discharge in argon gas (operating pressure $P_o \leq 1 \times 10^{-4}$ Torr) with density $n_s = 10^9 \rightarrow 10^{10}$ cm^{-3} and $T_e \approx 2$ eV. The ionizing electrons are trapped by surface multidipole magnetic fields in the region closed to the filaments so that they cannot reach the target chamber and produce plasma there directly. We have also confined our study on double layers with $\phi \leq 10$ V. These procedures ensure that ionization effects are minimized in our double layer experiment. A schematic of the triple plasma device is shown in Figure 1.

Stable double layers with $\phi \leq 5\ T_e/e$ can routinely be achieved using the boundary conditions shown in Figure 2. We chose to investigate these smaller double layers in order to limit the accelerated electron beam energy to below the ionization potential of argon. From the boundary conditions shown in Figure 2, we expect ions to only come from the high potential source. These ions are usually pre-accelerated into the target chamber by the potential difference between the high potential source plasma and the target plasma. These ions are further accelerated by the double layer into the low potential side. These beam ions either exit the target chamber at the left boundary or they charge exchange with neutrals and form cold ions ($T_i \sim 0.3$ eV). The cold ions, once formed, are confined electrostatically by the potentials of grids B and C. Although the charge exchange reaction rate is relatively low at our operating neutral pressure, the cold ion density accumulates to a significant fraction of the beam ion density due to their long confinement times.

Electrons which enter the target chamber from the high potential source are those in the tail of the Maxwellian source distribution function. These electrons have almost no drift energy, thus becoming the thermal electron species in the target plasma. This contrasts with the situation at the low potential end. There the tail of the source distribution function, which is energetic enough to get over the barrier provided by grid A, is accelerated into the target plasma. This results in an electron drift with the drift energy determined by the potential difference between grid A and the target plasma.

The boundary conditions in this experiment are believed to play the following roles:

1. The high potential side boundary ensures that the ions will enter the target chamber with a flow velocity $u_o > C_s$. This situation is quite similar to that of a sheath at a plasma boundary. Downward curvature of the plasma potential requires an ion drift velocity $u_o > C_s$. Since the high potential side electrons can be treated as approximately isothermal, the "Bohm sheath criteria" applies in this case for the double layer as well.

2. Grid B acts as a potential barrier for the low potential source ions as well as for the charge exchange cold ions which formed between the double layer and grid B. Since the height of the potential barrier of grid B is roughly 20 times the ion temperature ($T_i \approx 0.3$ eV), no low potential source ions are expected to enter the target chamber. On the other hand, the high potential source ions are at a much higher energy than grid B and can exit through grid B into the low potential source. As such the only source of thermal ions in the target plasma appears to be that of the charge exchange ions.

3. The low potential side boundary allows only electrons to drift in from the left. Such excess electron space charge may be neutralized only by the ion beam and the charge exchange ions.

4. There is no externally applied electric field across the target plasma since grids B and C are at roughly the same potential. The formation of double layers is a result of the particle flow rather than that of an external electric field.

Using the experimental boundary conditions and the particle distributions at the sources, it is possible to determine the potential profile across the target chamber by solving the Vlasov-Poisson equations. The details of such calculations have been described in an earlier paper (Hershkowitz et al., 1981) and will not be repeated here. Rather we will point out some results which are relevant to our present discussion. A typical solution of the target plasma potential profile and the boundary conditions employed is shown in Figure 3. The model has grid potentials similar to those shown in Figure 2. The double layer is formed in the region $x_L \leq x \leq x_R$ where $\phi(x_L) = 0$ and $\phi(x_R) = \phi_D$. Using the dimensionless variable $\psi = e\phi/T_e$, the density of the free ions n_{if} and trapped electrons n_{et} entering from the high potential source are, respectively:

$$n_{if}(\psi) = \frac{N}{2} e^{(T_e/T_i)(\psi_2-\psi)} \operatorname{erfc} \sqrt{\frac{T_e}{T_i}(\psi_2 - \psi)} \tag{1}$$

and

$$n_{et}(\psi) = N e^{(\psi-\psi_2)} (1 - \operatorname{erfc}\sqrt{\psi - \psi_A}) \quad . \tag{2}$$

The density of the free electrons entering from the low potential source is:

$$n_{ef}(\psi) = \frac{N}{2} e^{\psi-\psi_1} \operatorname{erfc}\sqrt{\psi - \psi_A} \tag{3}$$

where ψ_1, ψ_2 and ψ_A are, respectively, the low potential source, high potential source, and grid A potentials normalized to the electron temperature. Both source particles are assumed to be Maxwellian distributed with equal density N.

The density of the charge exchange ions cannot be calculated from the boundary conditions, thus it can be treated as a variable or:

$$n_{it}(\psi) = \beta\, n_e(0)\, e^{-(T_e/T_i)\psi} \tag{4}$$

and

$$\beta = 1 - \frac{n_{if}(0)}{n_e(0)} \quad . \tag{5}$$

β is a parameter which depends on the density ratio of the trapped ions to the beam ions and $n_e(0)$ is the total electron density at $\psi = 0$.

We show the dependence of the double layer on the trapped ion density with β varying from 0 to 0.35 in Figure 4. As the trapped ion density increases, the double layer becomes more detached from the low potential side boundary. Since $\beta = 0.35$ corresponds closely to the potential profile in the experiment, it is possible that a significant amount of charge exchange ions are trapped by the double layer at the low potential side; i.e., $\beta = 0.35$ corresponds to a trapped ion/beam ion density ratio of 54 percent. The trapped ions neutralize the excess negative space charge created by the drifting electrons, thus maintaining a uniform plasma potential at the low potential region of the double layer.

The contributions of the various particle species on the double layer space charge are shown clearly in Figures 5a and 5b where the charge density profile and particle density profiles are plotted versus axial distance. As discussed earlier, the ion beam provides the positive charge density for the downward curvature of the double layer at the high potential side, while the drifting electrons supply the negative charge density for the upward curvature of the double layer at the low potential side.

III. THE FORMATION MECHANISM

In order to understand the triggering mechanism for the double layers in our experiment, we examine the temporal evolution of the target plasma potential profile with $v_D \leq v_{te}$ and $v_D > v_{te}$. An extra grid is installed at the low potential side to facilitate the pulsing of the drifting electrons. The boundary conditions for this experiment are shown in Figure 6. A steady state target plasma with $n_e \cong 10^7\ cm^{-3}$ is extracted from the high side source, and the target plasma potential is quite uniform axially with $\phi_T = 4$ V. Low side source electrons and ions are normally excluded from the target plasma by the potential barriers of grid B (biased at -30 V) and grid C (biased at +12 V), respectively.

At time t = 0, grid B is switched to the ground potential and the low side source electrons are accelerated into the target plasma by the potential difference between ϕ_T and ground, i.e.,

$$v_D \cong \sqrt{\frac{e\,\phi_T}{T_e}}\, v_{te} \quad . \tag{6}$$

When the un-neutralized electron stream enters the target plasma, the entire target potential decreases rapidly from 4 to 3 V in 10 μs which results in $v_D = 1.2\ v_{te}$. The temporal evolution of the target plasma potential profiles, as obtained with an emissive probe using Boxcar interferometer averaging technique, is shown in Figure 7. A potential well begins to form near the electron injection boundary at t = 50 μs. The potential well grows deeper and widens into a double layer at t > 400 μs. The amplitude of the double layer is $\phi = 1.1\ T_e/e$ and appears to be quite stable. This result can be interpreted as follows.

Electron injection from the low side source creates excess space charge at the injection boundary, and a virtual cathode-type potential well is formed to limit the injected current. The growth of the potential well is accompanied by ion trapping in the potential well. As the density of the trapped ions increases, the double layer becomes detached from the electron injection boundary, in agreement with our earlier result on the effects of trapped ions (see Figure 3). Notice the double layer formation time of $T_{DL} \leq 400$ μs is considerably shorter than the charge exchange time of $T_{cx} \cong 1$ ms in this experiment. At such, the trapped ion population cannot come entirely from the charge exchange ions which fall into the potential well. A more possible source is the neighborhood ions which fall into the well during its growing phase. These ions will actually get accelerated down the potential well with energies depending on their locations in the potential well.

We further decrease the drift velocity of the injected electrons by decreasing the target plasma potential to $\phi_T \cong 3$ V. When the un-neutralized electron stream enters the target plasma, ϕ_T decreases from 3 to 1.5 V in 10 μs. As shown in Figure 8, a potential well is once again formed near the electron injection boundary at t = 50 μs when $v_D \cong 0.7\ v_{te}$. At t > 75 μs, a small double layer with $\phi \cong 0.5\ T_e/e$ has formed. However, in contrast with the earlier experiment, the double layer decays into an ion hole-like potential well. Note the similarity between the potential profile at t = 150 μs and an ion-acoustic double layer.

The time history of the plasma potential (ϕ_L) at an axial distance of x = 10 cm, the electron current flow across the target chamber from the low potential source (I_{eH}), and the ion saturation current (I_{iL}) at x = 15 cm are shown in Figure 9 in order to illustrate the double layer formation processes. At t > 50 μs, $\phi_T = 1$ V, and $v_D \cong 0.7\ v_{te}$, the growth of the potential well corresponds to the abrupt decrease of ϕ_L. On the other hand, I_{eH} continues to increase due to the injected electron current until ϕ_L becomes negative where I_{eH} begins to decrease rapidly. As ϕ_L reaches a minimum at -1.0 V, I_{eH} returns almost to the level at t < 0. ϕ_L subsequently becomes slightly more positive, and an intense low frequency noise appears in I_{iL} which corresponds to the evolution of the ion hole-like pulse.

A similar evolution process is observed when we increase v_D just slightly. As shown in Figure 10, the double layer breaks into one or more ion hole-like pulses. The long time history of this experiment is shown in Figure 11. The ion saturation current exhibits relaxation-type oscillations in time with a period roughly characterized by the transit time of the ion hole-like pulses across the target plasma. The relaxation oscillation corresponds to the evolution of the double layer from virtual cathode potential well and the subsequent decay into ion hole-like pulses. When the pulses reach the high side boundary (e.g., the ion-hole velocity is the order of the ion thermal velocity), the process repeats itself.

The breaking of the double layer into the ion hole-like pulses can be understood as follows. The magnitude of the virtual cathode potential well ϕ_w is formed to limit the injected current. Since the potential well must become a potential barrier to the injected electrons in order to limit the current, $\phi_w \cong (v_D/v_{te})^2 T_e/e$. The potential drop of the double layer $\phi \cong \phi_w$; also, we have $\phi = (v_D/v_{te})^2 T_e/e$.

As shown in Figure 9c, the injected current I_{eH} and v_D are reduced to very small values as a result of the formation of the double layer. We believe the growth of the potential well and the double layer formation also triggered bursts of counterstreaming ions which are accelerated down each side of the potential well with an average velocity:

$$v_b < \sqrt{\frac{2e\phi}{T_e}}\, C_s \quad . \tag{7}$$

This results in a counterstreaming or "tuning fork" ion phase space configuration at the double layer front. As reported in many numerical and experimental studies (Pécseli and Trulsen, 1984; Chan et al., 1984) of ion-acoustic shocks and ion holes, the ion-ion two-stream region becomes unstable when $v_b \leq C_s$ and evolves into one or more ion phase-space vortices.

As we have observed double layer formation with $v_D \leq v_{te}$, it is doubtful that the Buneman instability plays any roles in triggering the formation of double layers in these experiments. When $v_D < v_{te}$, no steady double layer exists as a result of the ion two-stream instability and the evolution of ion phase-space vortices.

IV. DISCUSSION

We have reviewed results from a series of laboratory experiments concerning the formation of double layers in a triple plasma device. In steady state, the double layer electric field is sustained by the negative space charge of the drifting electrons and the positive space charge of the ion beam. The low potential boundary condition permits the injection of an un-neutralized electron species which space charge is crucial for the initiation of the virtual cathode potential well. The ion reflecting grid (grid B in Fig. 2) plays two roles; first, to prevent the low potential source ions from entering the double layer and second, to confine the charge exchange cold ions in the low potential side of the double layer. The charge exchange (trapped) ions are needed to neutralize part of the drifting electrons, thus allowing the double layer to move away from the low potential boundary.

The formation phase of the double layers is associated with the growth of virtual cathode-type potential wells at the electron injection boundary. The formation of the virtual cathode potential well is a result of the lack of neutralizing ions at the electron injection boundary. As long as the injected electron density is sufficiently high, the potential well will form independent of v_D and it need not be associated with instabilities. We have clearly shown the formation of double layers with $v_D < v_{te}$ which is below the threshold of the Buneman instability.

The movement of the double layer electric field away from the electron injection boundary is probably caused by the accumulation of the trapped ion density at the low potential side of the double layer as demonstrated by Figure 3. Since the double layer formation time is much shorter than the charge exchange time, the source of trapped ions is more likely coming from ions in the neighborhood of the potential well during the growth of the well. As such, these ions are accelerated down the potential well with a maximum velocity of:

$$v_b \leq \sqrt{\frac{2\, e\, \phi_w}{T_e}}\ C_s \quad . \tag{8}$$

When the magnitude of the potential well $\phi_w < T_e/e$, the ions become two stream unstable because $v_b < C_s$. As such, the double layer decays into ion phase space vortices with potential structures that resemble ion acoustic double layers. This situation is similar to the auroral plasma condition where small electric signatures (Temerin et al., 1982) are often observed along with counterstreaming ions.

For the case of $v_D > v_{te}$, the depth of the potential well $\phi_w > T_e/e$ and results in a stable double layer formation. For the stable double layers, the charge exchange ions will be the main fueling source for the trapped ion population in steady state. In that case, the main loss mechanism for the trapped ions is radial diffusion to the side walls.

Acknowledgments. The authors wish to thank N. Hershkowitz, G. Payne, H. Pécseli, J. Juul Rasmussen, H. Schamel, M. Silevitch, and S. Torvén for valuable discussions. This work was supported in part by NSF grant 83-14488.

REFERENCES

Chan, C., M. H. Cho, N. Hershkowitz, and T. Intrator, *Phys. Rev. Lett., 52,* 1782 (1984).
Hershkowitz, N., G. Payne, and C. Chan, *Plasma Phys. 23,* 910 (1981).
Hollenstein, Ch., M. Guyot, and E. S. Weibel, *Phys. Rev. Lett., 45,* 2110 (1980).
Iizuka, S., K. Saeki, N. Sato, and Y. Hatta, *Phys. Rev. Lett., 43,* 1404 (1979).
Leung, P., A. Y. Wong, and B. H. Quon, *Phys. Fluids, 23,* 992 (1980).
Pécseli, H. L., and J. Trulsen, *Phys. Rev. Lett., 48,* 1355 (1982).
Pécseli, H. L., R. J. Armstrong, and J. Trulsen, *Phys. Rev. Lett., 81A,* 386 (1980).
Quon, B. H., and A. Y. Wong, *Phys. Rev. Lett., 37,* 1393 (1976).
Saeki, K., S. Iizuka, and N. Sato, *Phys. Rev. Lett., 45,* 1853 (1980).
Sato, T., and H. Okuda, *Phys. Rev. Lett., 44,* 740 (1980).
Singh, N., and R. W. Schunk, *Phys. Fluids, 26,* 2781 (1983).
Temerin, M., K. Cerny, W. Lotko, and F. S. Mozer, *Phys. Rev. Lett., 48,* 1175 (1982).

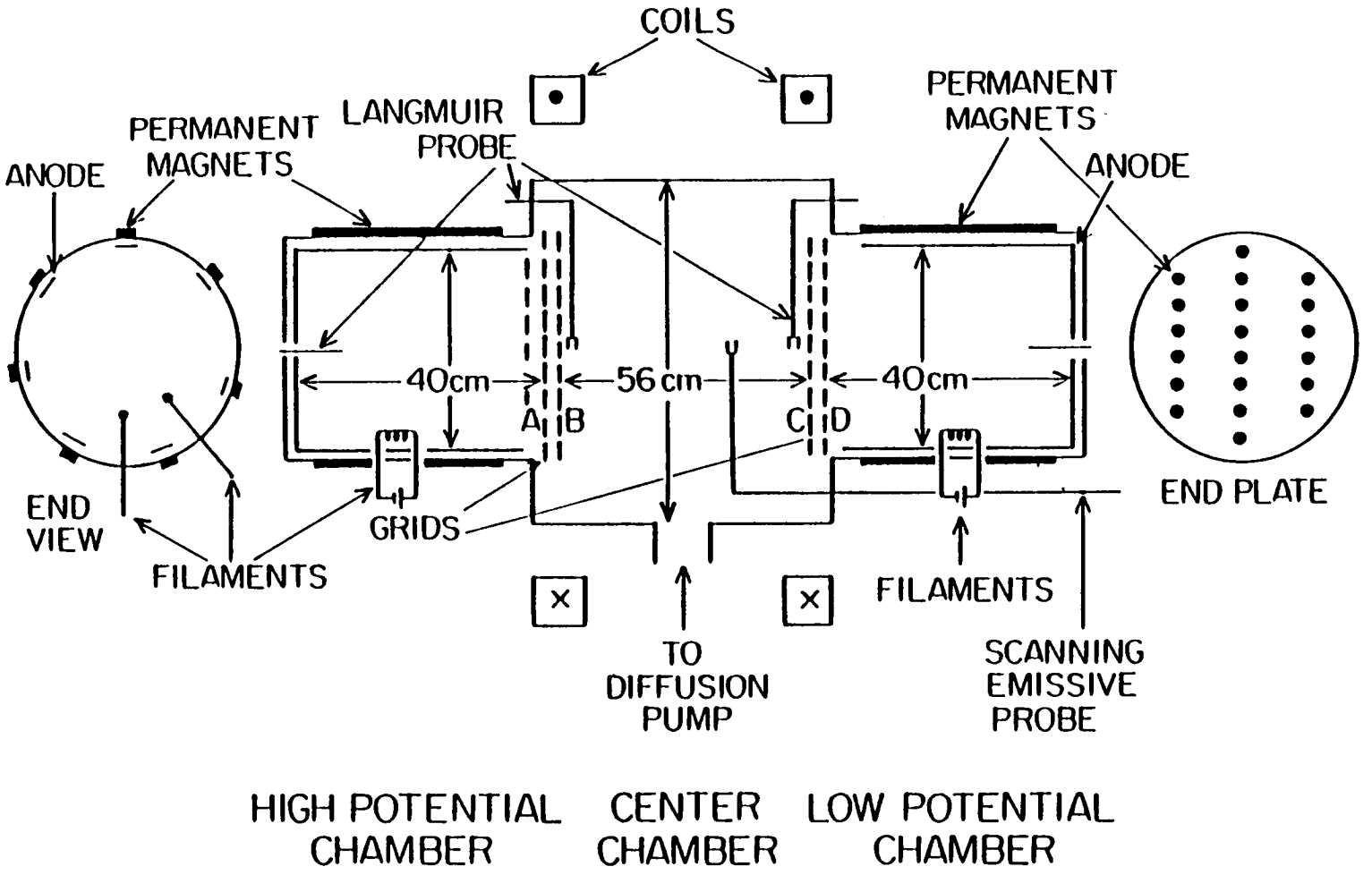

Figure 1. A schematic of the triple plasma device.

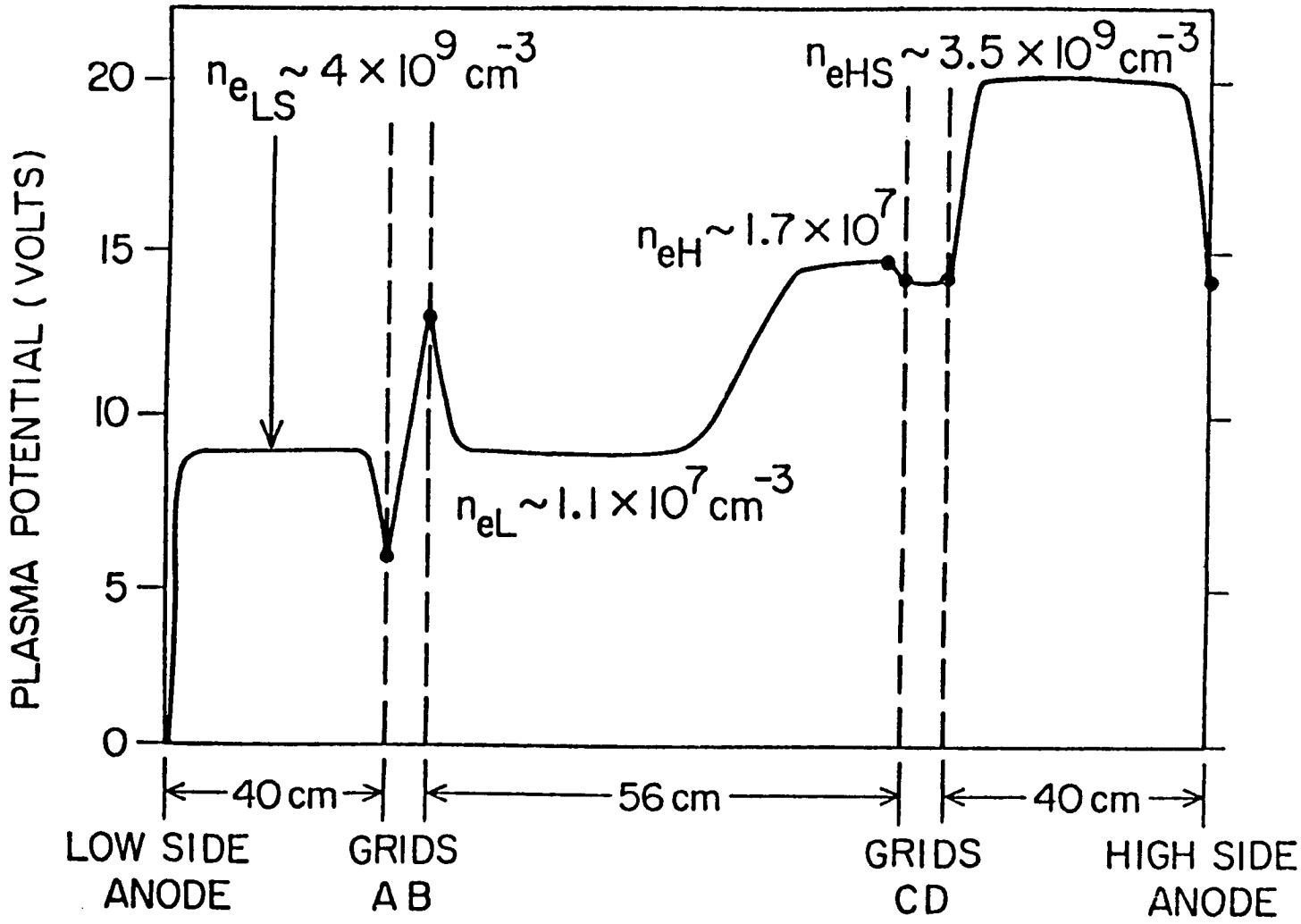

Figure 2. Axial potential profile of the laboratory double layer including the boundary condition.

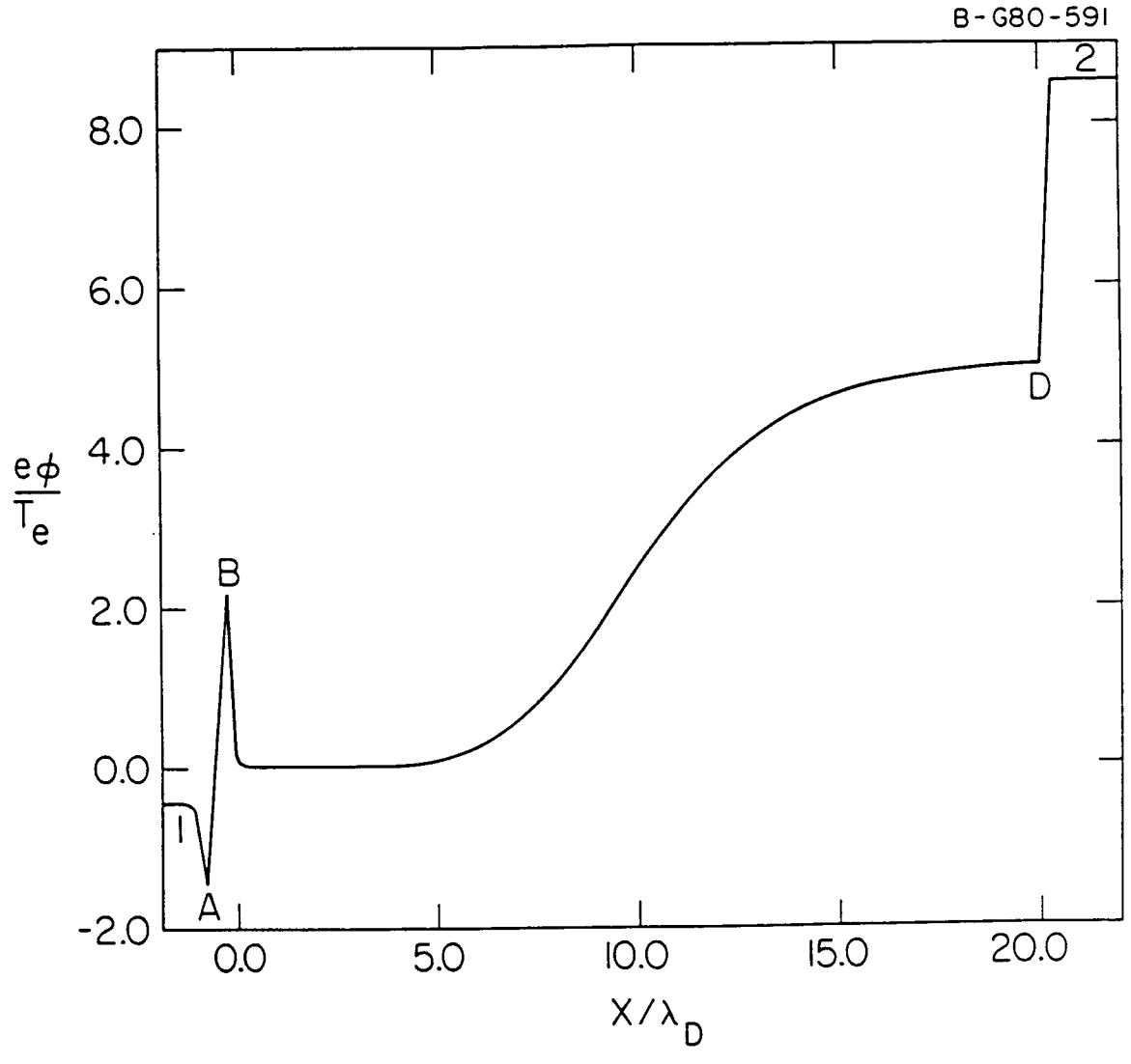

Figure 3. A solution of Poisson's equation $d^2\psi/dx^2 = n_{ef}(\psi) + n_{et}(\psi) - n_{if}(\psi) - n_{it}(\psi)$ where $\psi = e\phi/T_e$; $x = x/\lambda_D$; n_{if}, n_{et}, n_{ef}, and n_{it} are given by equations (1) through (4), respectively.

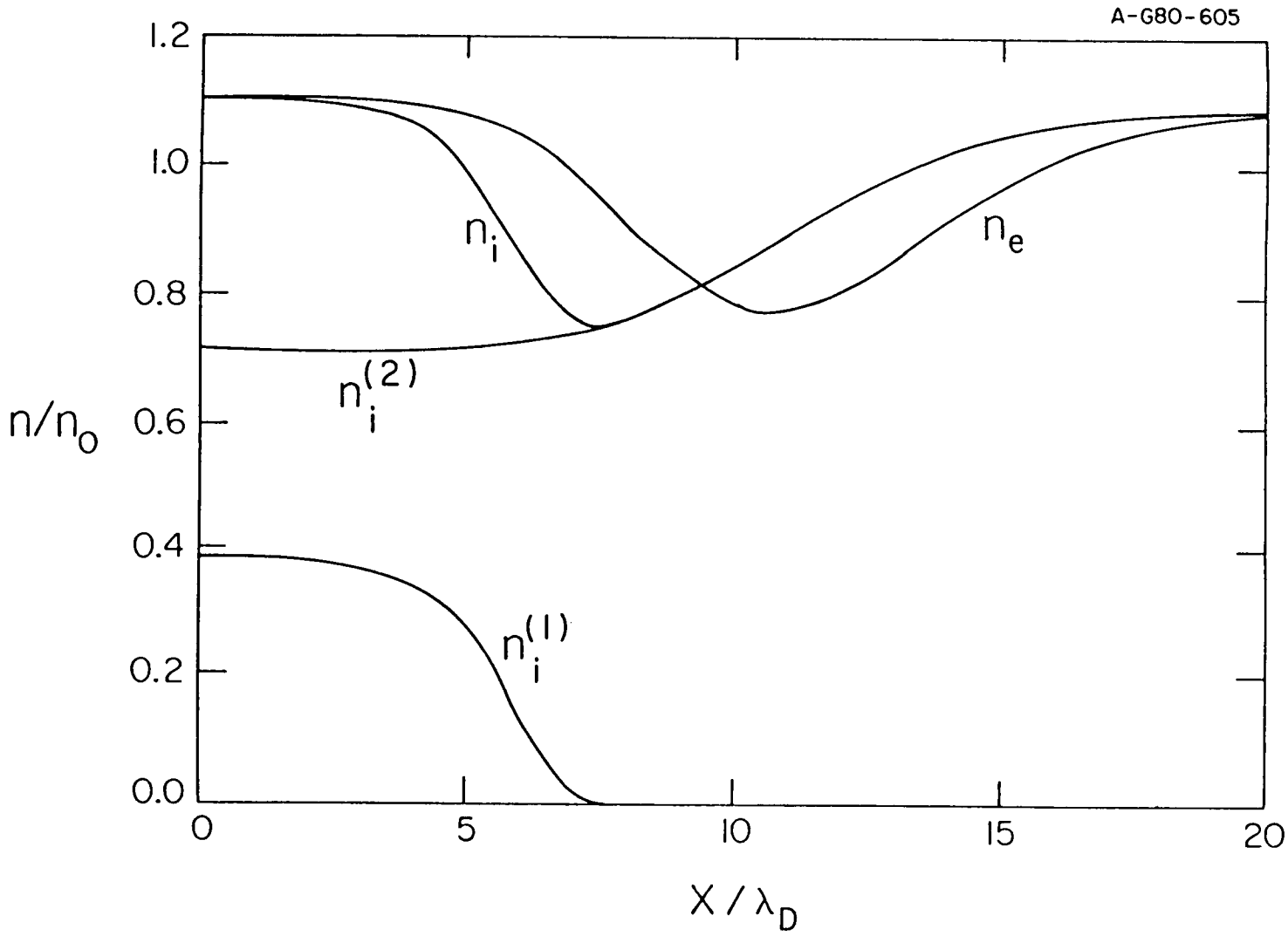

Figure 4a. The total ion and electron density profiles for the model double layer.

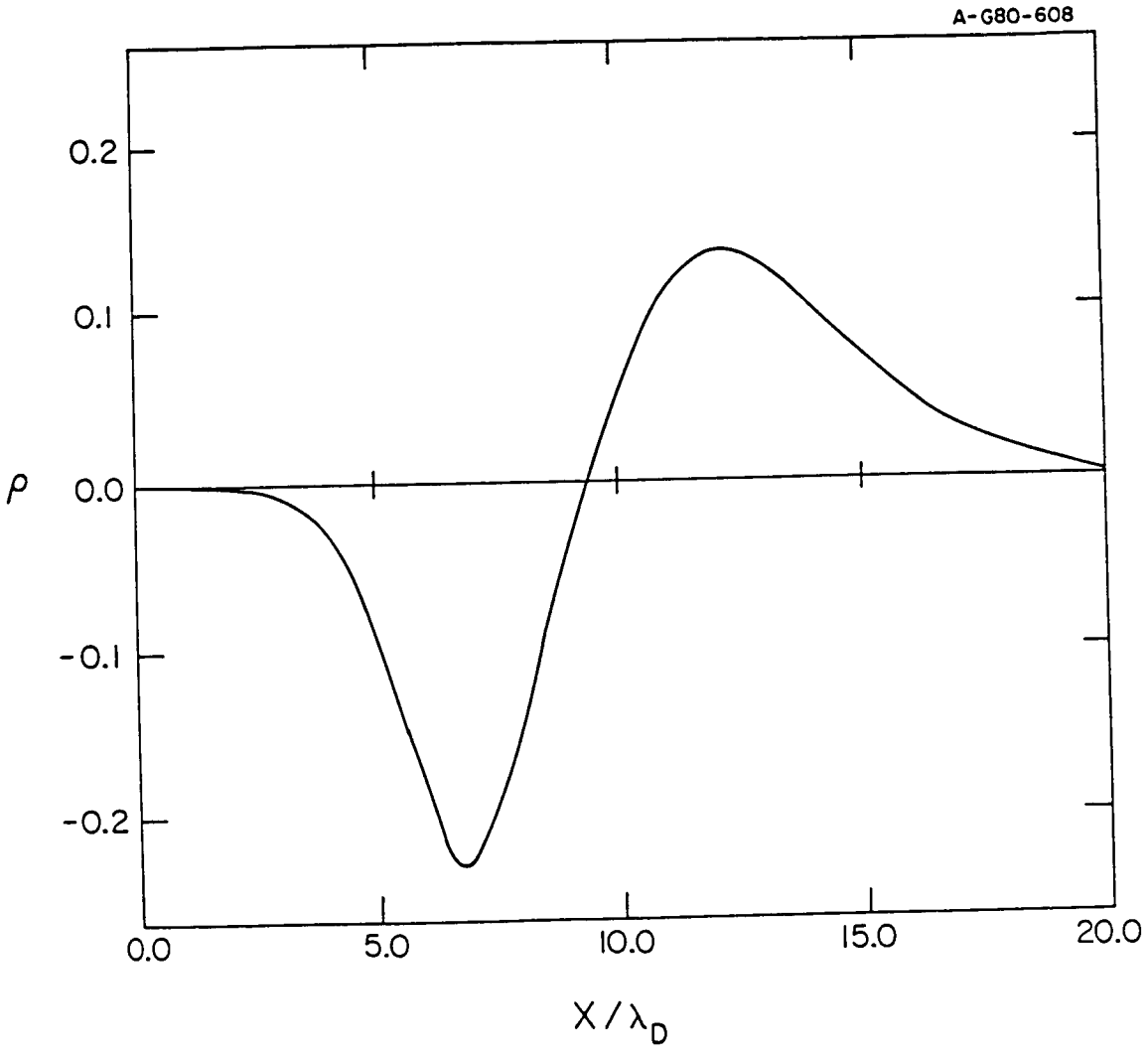

Figure 4b. Total charge density profile for the model double layer.

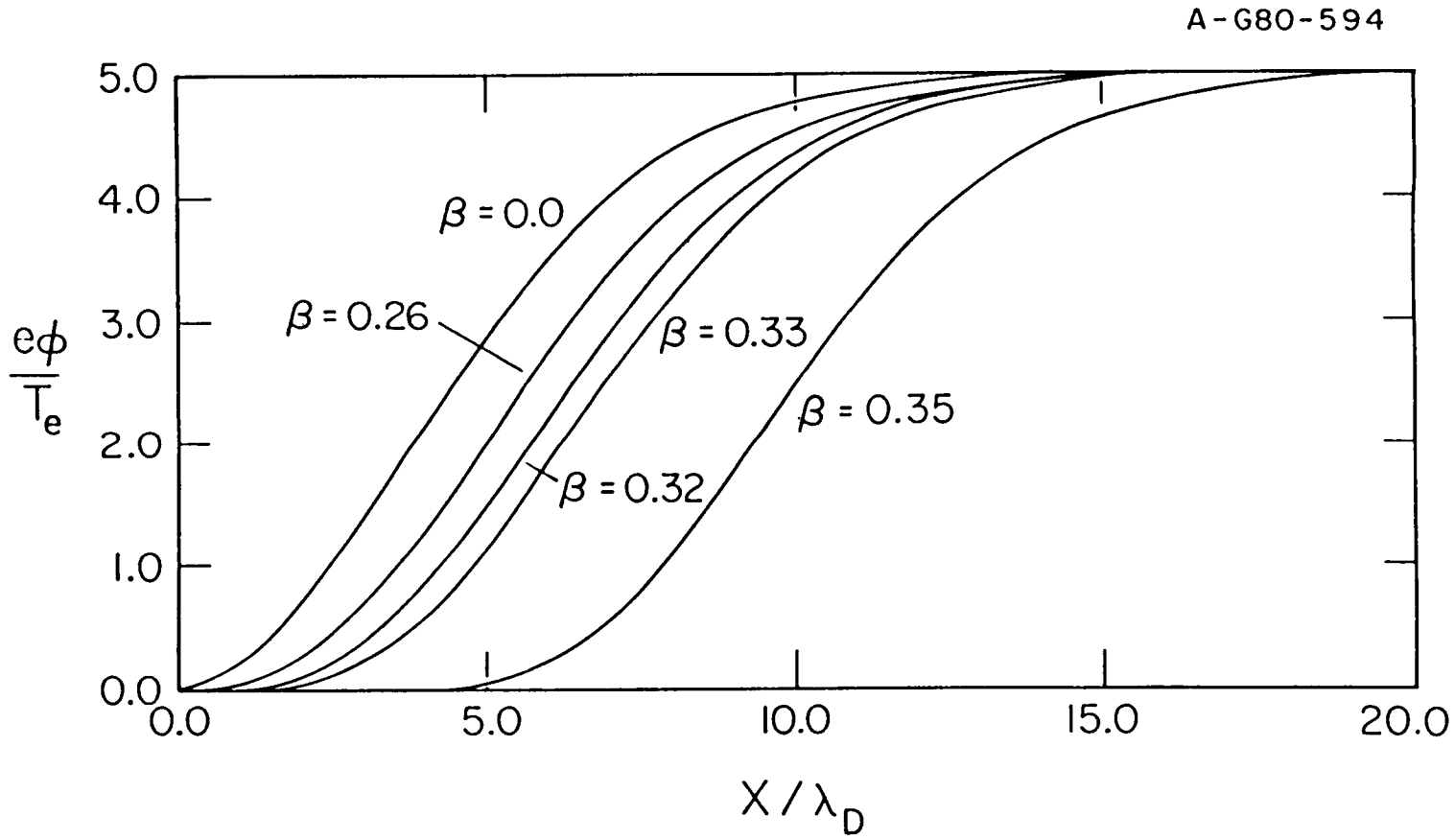

Figure 5. Illustration of the dependence of double layer position on the density of trapped ions. The curve labeled $\beta = 0.0$ has no trapped ions.

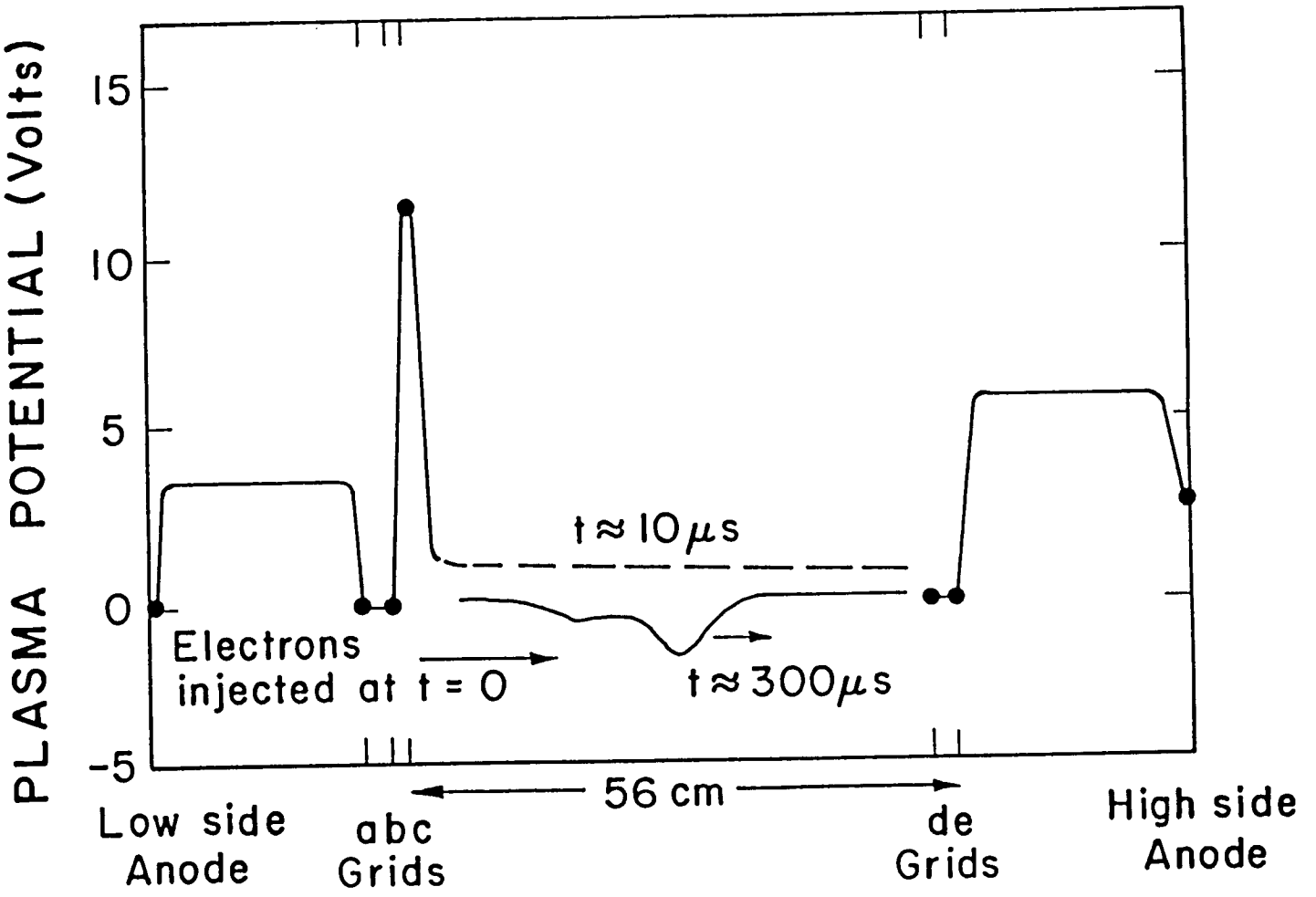

Figure 6. Axial potential profile along the axis of the device. Grid B was switched from -30 V to ground at t = 0.

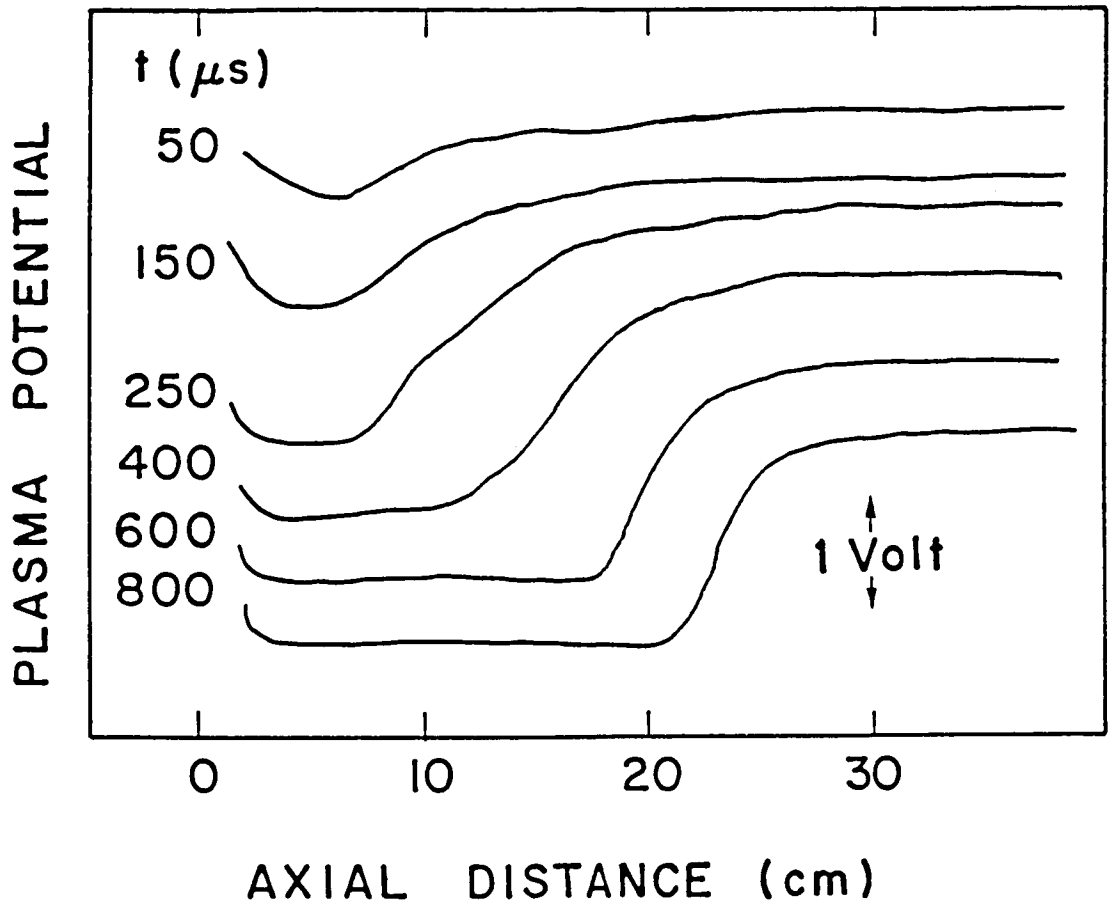

Figure 7. Temporal evolution of the target plasma potential profile when $v_D > v_{te}$. Each profile is displaced for clarity.

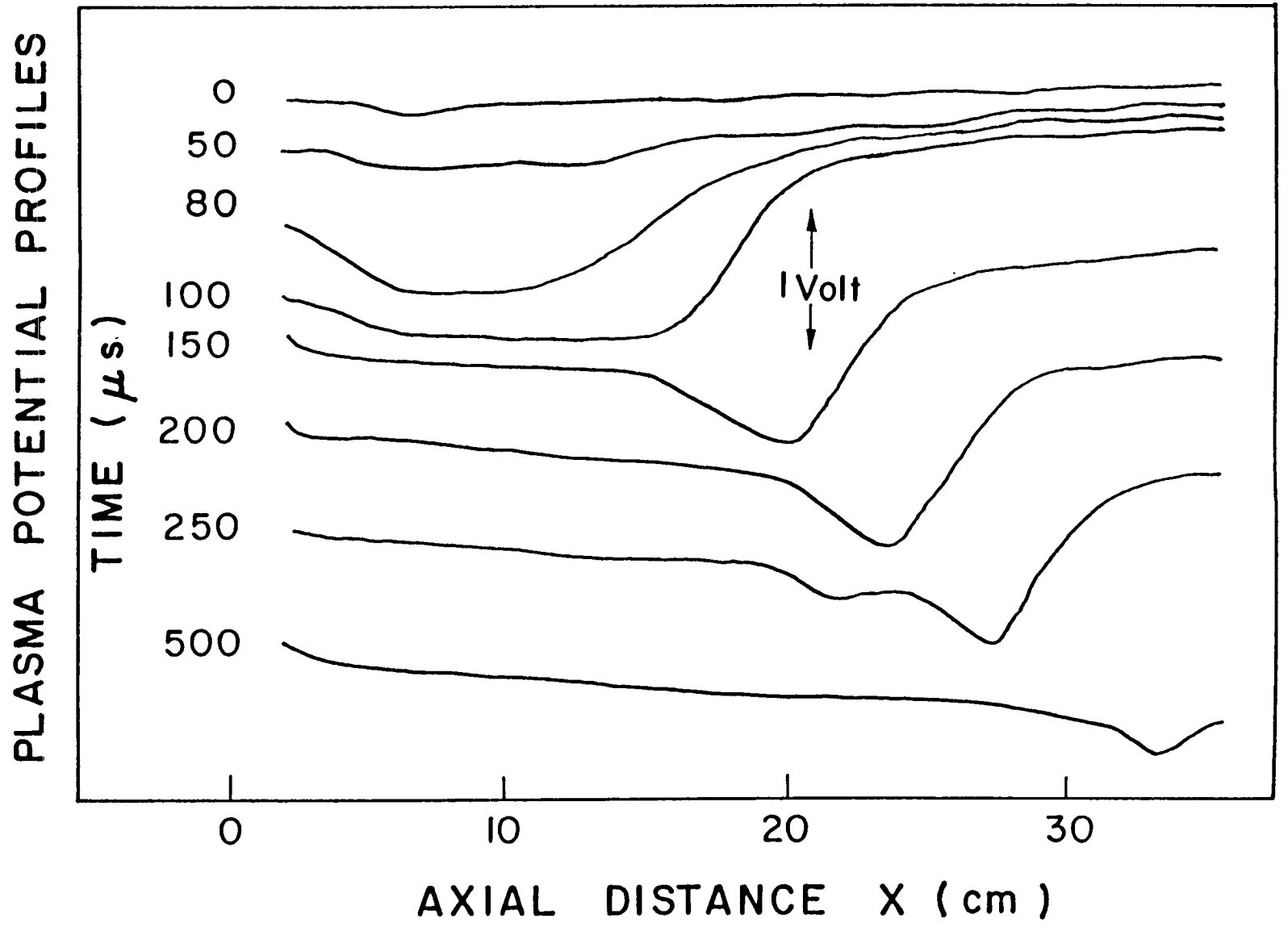

Figure 8. Temporal evolution of the target plasma potential profile when $v_D > v_{te}$.

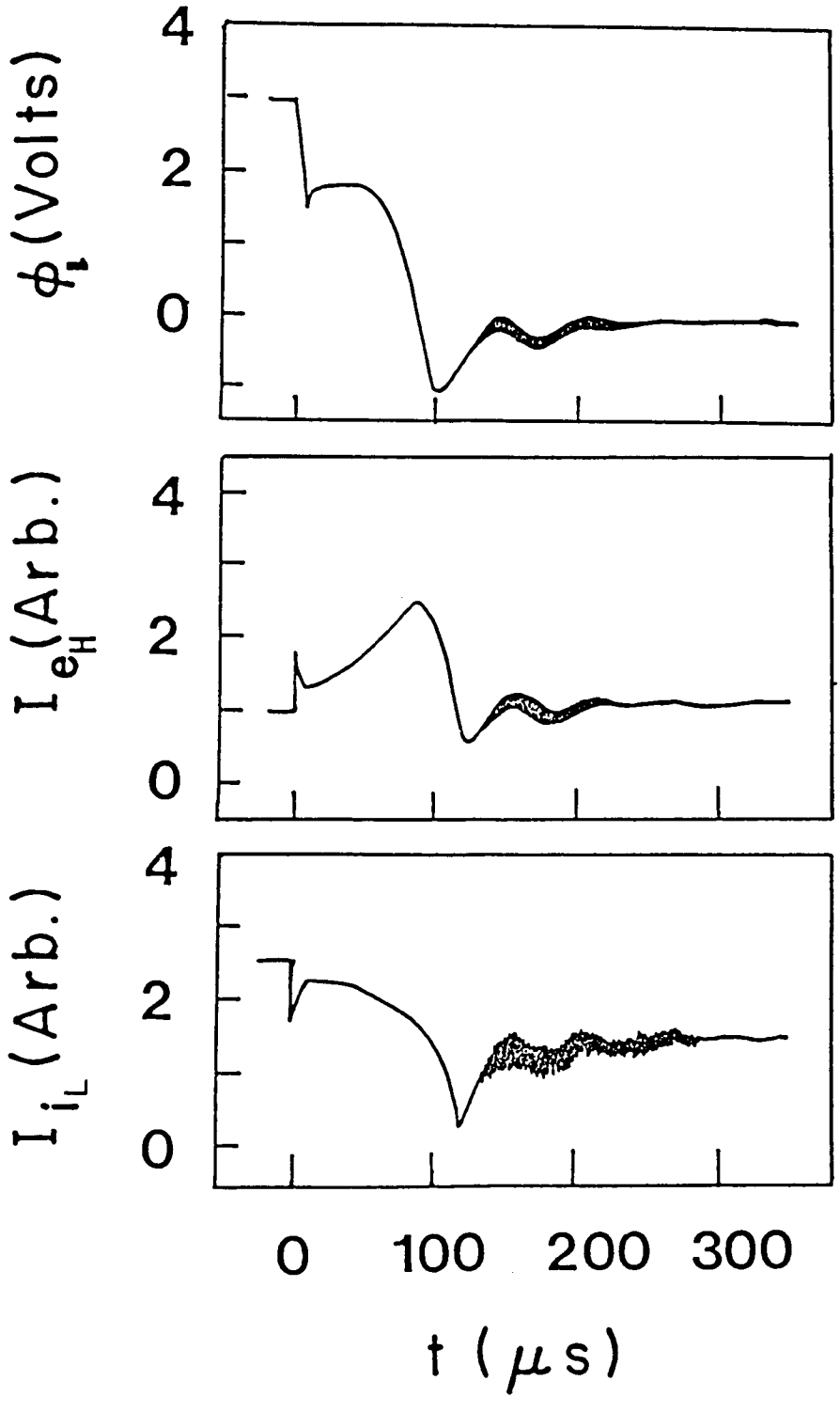

Figure 9. Time history of (a) the target plasma potential (ϕ_L) as measured by an emissive probe at 10 cm away from grid C; (b) the electron current (I_{eH}) collected by a single-sided Langmuir probe facing the low potential source; and (c) the ion saturation current (I_{iL}) collected by a wire probe at 15 cm away from grid C.

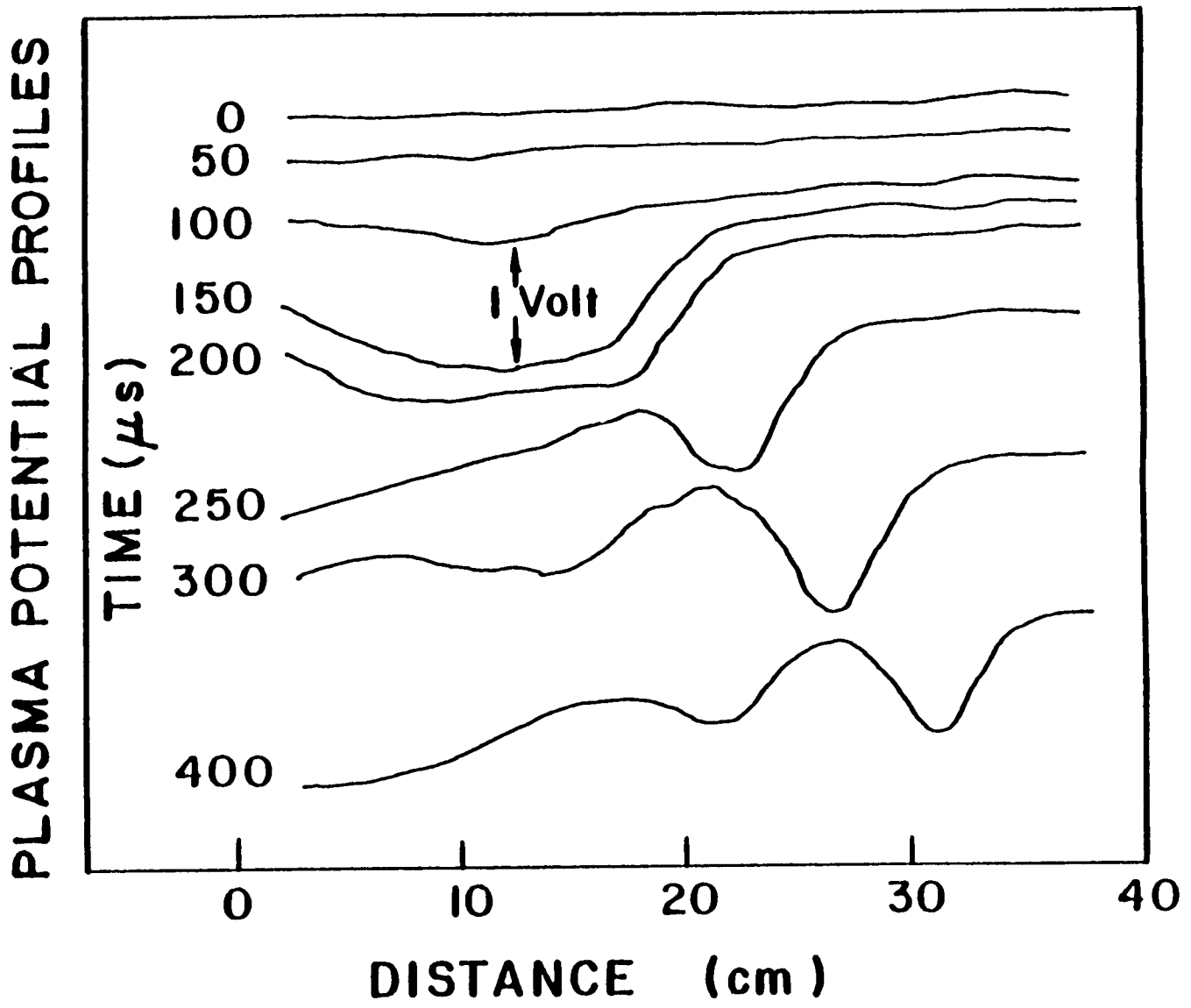

Figure 10. Temporal evolution of the target plasma potential with $v_D < v_{te}$ and the double layer decays into more than one ion hole-like pulses.

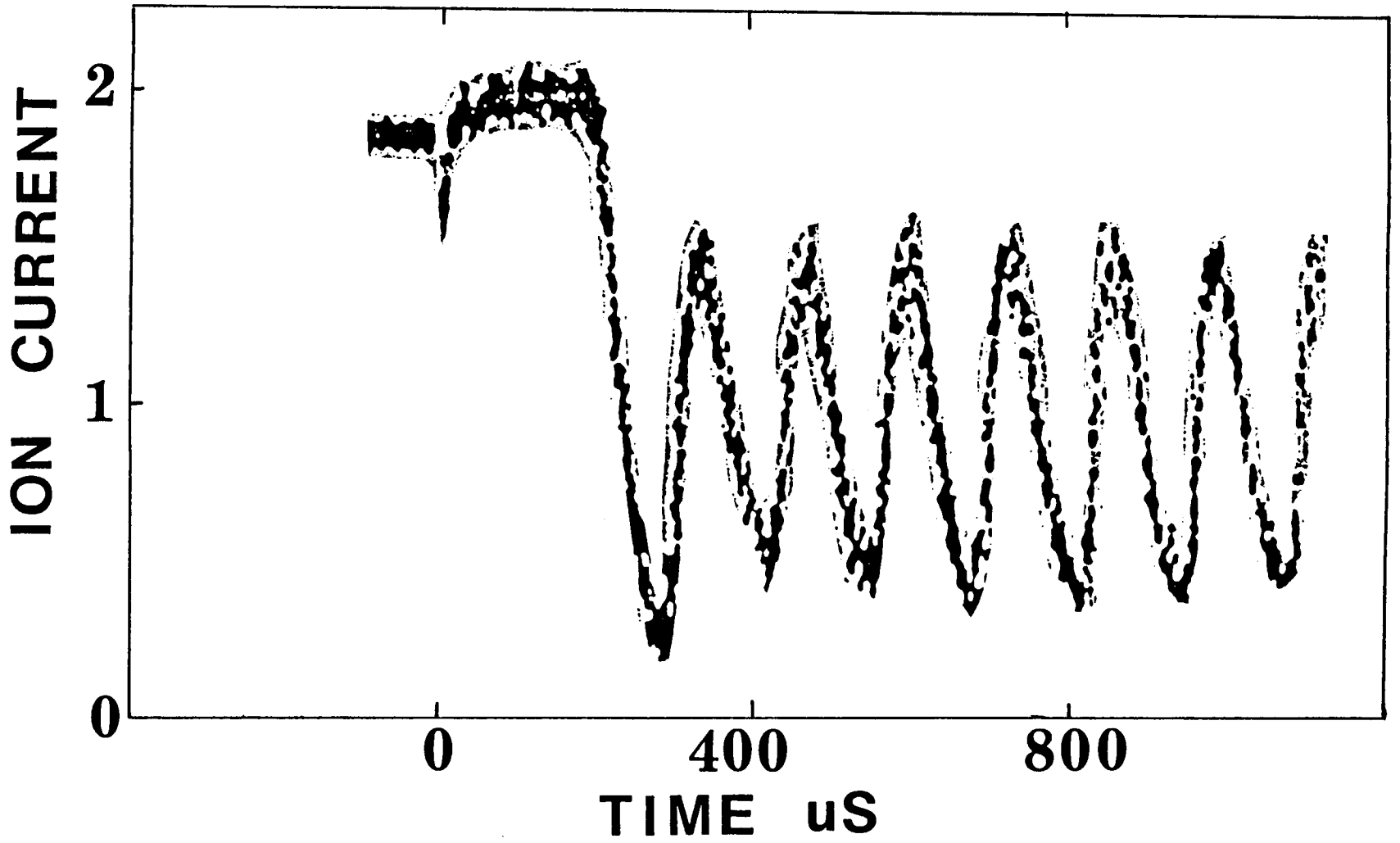

Figure 11. Long time history of the ion saturation current when the system exhibits relaxation oscillation.